Composites Science and Technology 203 (2021) 108563

Contents lists available at ScienceDirect

Composites Science and Technology

journal homepage: http://www.elsevier.com/locate/compscitech

# Porous bone tissue scaffold concept based on shape memory PLA/$Fe_3O_4$

Wei Zhao [a], Zhipeng Huang [b], Liwu Liu [a], Wenbo Wang [b], Jinsong Leng [c,**], Yanju Liu [a,*]

[a] Department of Astronautical Science and Mechanics, Harbin Institute of Technology (HIT), P.O. Box 301, No. 92 West Dazhi Street, Harbin, 150001, China
[b] The First Affiliated Hospital of Harbin Medical University, No. 23 You Zheng Street, Harbin, 150001, China
[c] Center for Composite Materials and Structures, Harbin Institute of Technology (HIT), P.O. Box 3011, No. 2 YiKuang Street, Harbin, 150080, China

ARTICLE INFO

*Keywords:*
Smart materials
Shape memory behaviour
3D printing
Bone tissue scaffold

ABSTRACT

Bone tissue engineering is one of the important treatment methods for bone defects, especially relatively large bone defects. A variety of design strategies have been developed to obtain bone tissue scaffolds. The development of scaffolds equipped with more functions can provide more options for the treatment of bone defects, which, however, remains a challenge. Here, we introduce 3D printed porous bone tissue scaffolds based on shape memory polymer composite (SMPC). The designs are proposed based on thorough observation and analysis of the microstructure of lotus root and cellular co-continuous-like structures. Moreover, the addition of magnetic nanoparticles endows the scaffolds with the ferromagnetic domains, which opens up an opportunity to implant bone tissue scaffolds into the body in a contracted state and make them a perfect match. The experimental and micromechanical theoretical studies of the mechanical properties illustrate the reliability of the structures, while the biological experiments verify the biological activity and osteogenic effect of these scaffolds. The shape memory effect suggests potential advantages in minimally invasive surgery. These porous scaffolds based on SMPC are expected to be applied to the repair and regeneration of bone tissue.

## 1. Introduction

Bone defect is one of the most common clinical diseases, which means that the structural integrity is destroyed [1]. They can be triggered by trauma, infection, tumors, osteomyelitis surgery, and various congenital diseases, among others. For orthopedic surgeons, the reconstruction of large bone defects has been a huge challenge [2]. Generally, the autologous bone graft is regarded as the "gold standard" to treat bone defects. However, the limited availability and donor site morbidity greatly limit the application of this method. Moreover, other treatments accompany problems of secondary injury, the spread of disease and immunological rejection. Given these limitations, bone tissue engineering, with characteristics of extensive sources, no obvious immune rejection response, and no damage to healthy bone structure, has emerged as an alternative for the treatment of bone defects [3–6].

Some key characteristics of biomedical scaffolds are essential for the successful repair of bone defects. Firstly, the scaffolds must be in close contact with the adjacent bone tissue to achieve osseointegration. Secondly, the scaffolds should be bioactive and osteoconductive to permit the migration of cells and facilitate integration with surrounding bone tissue. At present, many design strategies have been developed to fabricate the scaffolds [7–9]. However, some problems are still unavoidable in these scaffolds, including poor biocompatibility, low preparation efficiency, weak mechanical property and low porosity. Many scaffolds are fabricated by hydrogel, but the lack of mechanical strength and uncertain curing time usually results in the poor marginal contact between the scaffold and the bone defect. The cytotoxicity of some monomers or catalysts used for the preparation of hydrogels cannot be ignored. The typical in-situ hydrogel scaffolds lack adequate porosity and interconnected channels, which limits the rate of cell migration and the biodegradation of the hydrogel. Moreover, for the scaffolds fabricated by the bioactive ceramics or glass-ceramics, the brittle mechanical properties and low pore connectivity will greatly limit its application.

Consequently, bone tissue scaffolds based on shape memory polymer (SMP) with the "self-fit" function are designed and fabricated to repair the bone defect. SMP is a type of intelligent material with active deformation capability, which can take on a different shape than its original and recover to its initial shape stimulated by heat, electricity, magnetism, or light [10–19]. Because of the excellent biodegradability, biocompatibility and the unique shape memory effect, SMP (such as

* Corresponding author.
** Corresponding author.
*E-mail addresses:* lengjs@hit.edu.cn (J. Leng), yj_liu@hit.edu.cn (Y. Liu).

https://doi.org/10.1016/j.compscitech.2020.108563
Received 17 June 2020; Received in revised form 27 September 2020; Accepted 14 November 2020
Available online 25 November 2020

**Acronyms**

| | |
|---|---|
| CCK-8 | Cell Counting Kit-8 |
| ALP | Alkaline phosphatase |
| Runx2 | Runt-associated transcription factor 2 |
| OCN | Osteocalcin |
| OPN | Osteopontin |
| ECM | Extracellular matrix |
| RT-PCR | Real-time Polymerase chain reaction |
| PLA | Polylactic acid |

be implanted into the lesion site through minimally invasive surgery and self-fit the bone defects. Scaffolds with different porosities are fabricated by 3D printing technology [22,26–29]. A micromechanical theoretical study is developed to obtain the analytical solutions of mechanical properties changing with the temperatures and porosities, which provides the mechanical basis for the design of scaffolds. The finite element analyses, together with the functional verification experiments, verify the feasibility of this method and serve as an important basis for the minimally invasive implant. Experiments including the cell Counting Kit-8 (CCK-8), Real-time Polymerase chain reaction (RT-PCR) verify the cell attachment, proliferation, and gene expression effect of the scaffolds.

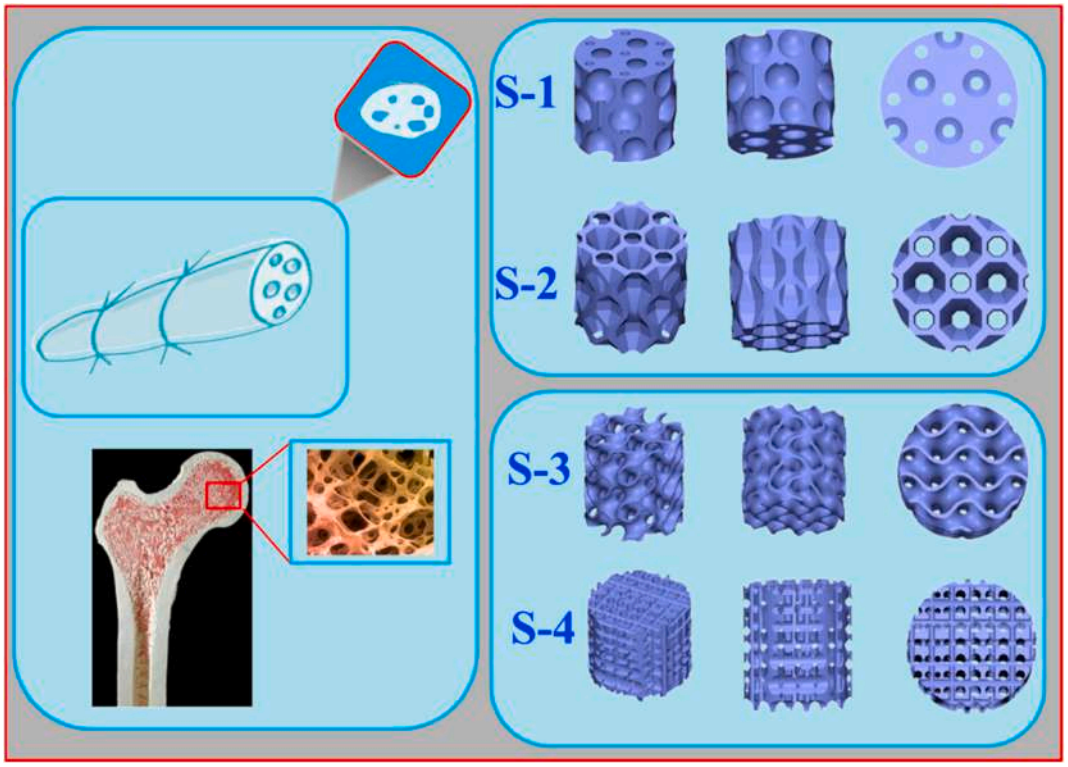


**Fig. 1.** Through the observation and analysis of lotus rhizomes structure and bone trabecular structure, the design schemes of the porous scaffold (S-1, S-2, S-3 and S-4) are proposed. 3D images of S-1with circular holes, S-2 with polygonal pores, S-3 with random non-direction pores, and S-4 with random orientation pores.

shape memory polyurethane, shape memory polylactic acid, shape memory polycaprolactone and their mixture) has attracted more and more attentions in biomedical applications, including tissue engineering, shape-morphing scaffolds, self-unfolding flexible microelectrode arrays, etc [20–25]. For example, the SMP based shape-morphing scaffold developed by Du et al. can transform from planar shapes to small-diameter tubular shapes [24]. This method shows great potential in the design of complex cellular scaffolds that mimic the complex anatomical structures of tissues or organs. Similarly, for SMP based bone tissue scaffold, the merit lies in that it can be implanted into the body with a compacted state and deployed in vivo, which makes the implantation process safer and more convenient.

The porous structure system is necessary for the regeneration of bone tissue, while it needs to provide adequate strength to resist external load generated during motion. Therefore, it is critical to developing structures with high porosity and large specific surface area without losing its strength. In this paper, through the observation and analysis of the microstructure of lotus rhizomes and cellular co-continuous-like structures, we propose a series of SMPC based bone tissue scaffolds that can

## 2. Results and discussion

### 2.1. Design strategy

Ideal bone tissue scaffolds should be equipped with appropriate porosity, suitable aperture size, and interconnected channels to promote cell adhesion, tissue formation and nutrients transmission [30–32]. Natural bone structures have the characteristics of strong but not brittle, hard but flexible, lightweight but efficient. By analyzing the porous structure of lotus rhizomes and co-continuous cellular bone tissue, four scaffolds, scaffold-1 (S-1), scaffold-2 (S-2), scaffold-3 (S-3), scaffold-4 (S-4), are proposed.

Lotus is a kind of aquatic plant with enlarged stems underground (rhizomes), which have many parallel channels distributing inside, as shown in Fig. 1(a). The paralleled multi-channels extend towards the lotus petioles, connect the lotus rhizomes to the leaves and create a clear space. The porous structures significantly expand the contact area, maintain the low flow resistance, promote the exchange of nutrients and reduce the weight of lotus rhizomes. Consequently, it is an ideal scaffold

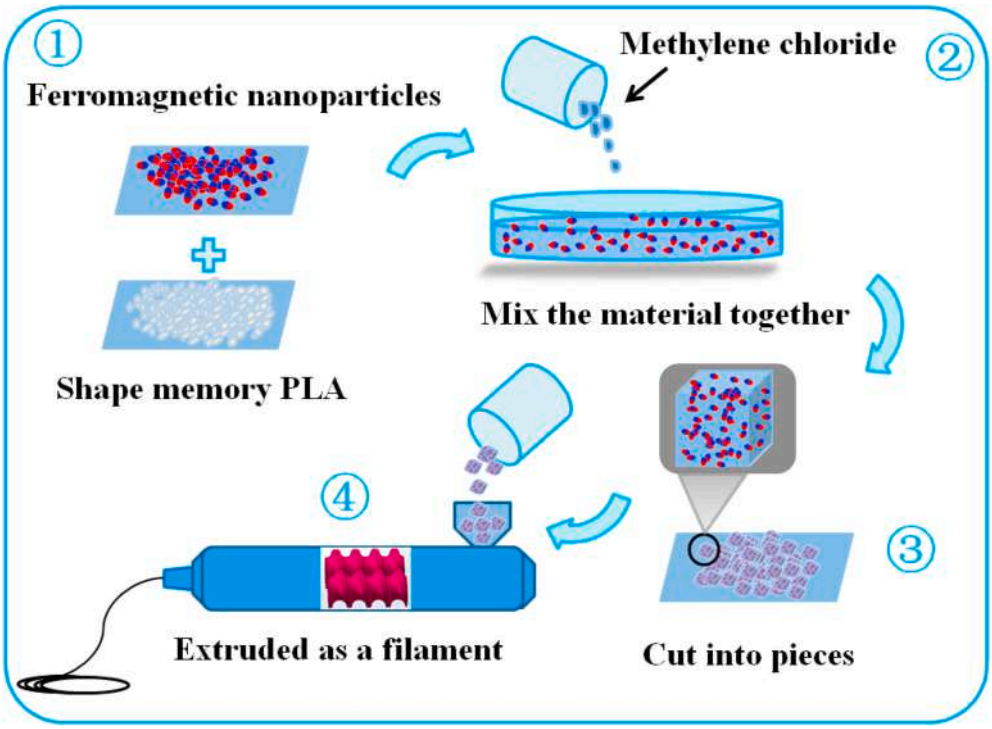


**Fig. 2.** Fabrication process of shape memory PLA/$Fe_3O_4$ filament.

model with low density, high porosity, and low flow resistance. Moreover, cancellous bone, a part of bone tissue, consists of interwoven rod-shaped or plate-like trabeculae, as shown in Fig. 1(d). Trabeculae have different arrangement directions, spacings, quantities, shapes, thicknesses, and other morphological characteristics, which connect each other to form porous network structures and exhibit different mechanical properties. The density, porosity, and strength of scaffolds are easier to design by adjusting the distribution of trabeculae. Consequently, by observing and analyzing the microstructure of lotus rhizomes and cancellous bone, four types of scaffolds (S-1, S-2, S-3 and S-4) were developed as shown in Fig. 1.

For S-1 and S-2, channels with different apertures were distributed on them along the longitudinal section direction and connected the ends of the scaffolds. Furthermore, channels along the transverse section direction were introduced to further increase the connectivity. It is worth mentioning that the porosity and mechanical strength of the scaffolds can be adjusted by regulating the element stacking method and number of channels. S-1 and S-2 are 12 mm in height and 12 mm in diameter with a porosity of 50%. Different shapes of pores are designed for the two scaffolds to investigate the different bioactivity and osteoconductive effect. S-1 has the spherical pores with aperture sizes ranging from 400 μm to 2.3 mm, while S-2 has the polyhedral pores with sizes ranging from 700 μm to 2.5 mm. After the scaffolds are implanted into the defect site, nutrients and cells can infiltrate into the interior of the scaffold along the channels. Channels with a large aperture can speed up the transportation of nutrients, while channels with a small aperture are beneficial to cell adhesion. Meanwhile, these pores endow the scaffolds with a large contraction ratio, which will facilitate the operation of the implant operation.

The scaffolds S-3 and S-4 are with a density of 60%, which are composed of trabecular like structure that interlaced together with varying sizes. The channels distribute uniformly and connect with each other to ensure adequate nutrient flow and avoid channel obstruction caused by cell accumulation. Scaffolds S-3 and S-4 are 12 mm in height with a diameter of 12 mm. The aperture sizes of the scaffold S-3 range from 600 μm to 800 μm, while the pore sizes of S-4 range from 400 μm to 600 μm.

### 2.2. Fabrication and morphological characterization

#### 2.2.1. Preparation of shape memory PLA with ferromagnetic domains

In this work, we use the shape memory polylactic acid/$Fe_3O_4$ to fabricate the porous scaffolds. Referring to scaffolds fabricated by Aleš Gregor et al. [7], the results indicate that polylactic acid-based scaffolds exhibit excellent biocompatibility and degradation. The ester bonds of shape memory polylactic acid can be hydrolyzed to produce lactic acid that generally presents in the body [33]. Adding magnetic nano-particles into SMP can realize remote non-contact drive, which has been widely used in many biomedical applications and verified by many experiments in vitro and in vivo [34–37].

The fabrication process of the shape memory polylactic acid/$Fe_3O_4$ used for 3D printing follows the steps shown in Fig. 2. The shape memory PLA was synthesized by the Center for Composite Materials and Structures, Harbin Institute of Technology. Firstly, 80 wt% shape memory PLA and 20 wt% $Fe_3O_4$ was sufficiently mixed and obtained a solid mixture. Subsequently, the solid mixture was fed into the twin-screw extruder (Cte20, Coperion Keya Machinely Co. Ltd) to obtain the shape memory PLA/$Fe_3O_4$ filament with a diameter of 1.75 mm. The mechanical properties of shape memory PLA/$Fe_3O_4$ composites can be found in Supporting Information S1-S3.

#### 2.2.2. Morphological characterization

An ANYCUBIC 3D printer (i3 MEGA) with a nozzle size of 0.4 mm was employed to fabricate the scaffolds. Fill density was set to 10% to further reduce the weight of the scaffolds. The scaffolds with the porosity of 50% (S-1 and S-2) and 60% (S-3 and S-4) are shown in Fig. 3 (a). Micro-CT scanning images are presented in Fig. 3(b) to show the printing resolution of the scaffolds. The interconnected channels of scaffolds S-1 and S-2 and the trabecular-like structure of scaffolds S-3 and S-4 can be clearly seen from the scanning images. The cross channels interconnect with the longitudinal channels in scaffolds S-1 and S-2, while trabecular like network interconnect to each other in scaffolds S-3 and S-4, which is consistent with the initial design.

The porosities of the scaffolds were determined by the drainage method (More details can be found in Supporting Information S4). The

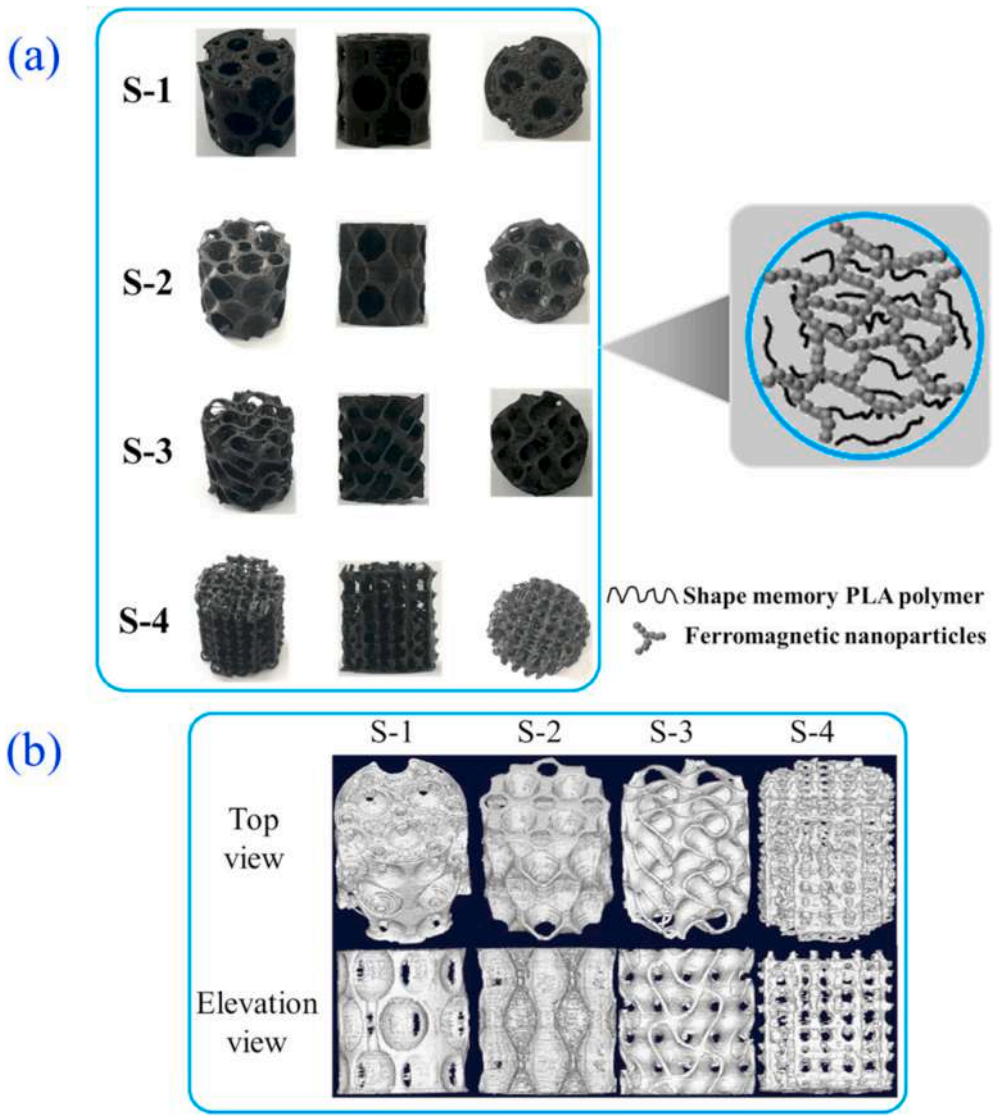


**Fig. 3.** Morphological characterization (a) Display of the printed scaffolds (b) Micro-CT scanning of S-1 (50% porosity), S-2 (50% porosity), S-3 (60% porosity) and S-4 (60% porosity).

**Table 1**
Physical parameters and the pore morphology.

| Type | Mean mass (g) | Volume ($mm^3$) | Porosity (%) | Pore interconnectivity (%) |
|---|---|---|---|---|
| S-1 | 1.2475 | 1356.78 | 50.28 ± 1.47 | 100 |
| S-2 | 1.3088 | 1356.78 | 50.37 ± 1.35 | 100 |
| S-3 | 0.9834 | 1356.78 | 60.73 ± 1.68 | 100 |
| S-4 | 1.0765 | 1356.78 | 60.36 ± 1.59 | 100 |

Microstructural characteristics and the pores morphology of the scaffolds are listed in Table 1. For the four types of scaffolds, the interconnectivity degrees of the pores is 100%. The high degree of pore interconnectivity has important functions not only on promoting the adhesion and migration of the cell, but also facilitating the efficient transport of oxygen/nutrients and metabolic wastes.

### 2.3. Mechanical property

Except for filling the bone defects to induce the growth of bone tissue, the scaffolds should provide enough support to withstand the force generated during normal walking. When people are walking, the reaction force of the ground on the foot is 1.5 times the body weight. Taking the femur as an example, the diameter of the femur is 6–10 cm. Generally, for an adult with a weight of 60 Kg, the thinnest place of the femur is about 6 cm. Therefore, for a scaffold implanted in this site, it will bear the stress of 0.21 MPa. If the safety factor is set to 1.2, the scaffolds can meet the mechanical requirement when the yield strength is greater than 0.252 MPa.

To investigated the compressive properties, the compression tests were conducted on a Zwick/Roell-010 universal testing machine with a test temperature of 37 °C. The compression strength of the four scaffolds changing with porosity is shown in Fig. 4(a). For the scaffolds with the porosity of 40%, 50%, 60%, and 70%, the compression strength is around 43 MPa, 32 MPa, 25 MPa, and 10 MPa, respectively, which is consistent with those obtained by the micromechanical differential method (Supporting Information S2). Additionally, according to the testing results, the compressive strength of scaffolds S-1 and S-2 is superior to that of scaffoldsS-3 and S-4.

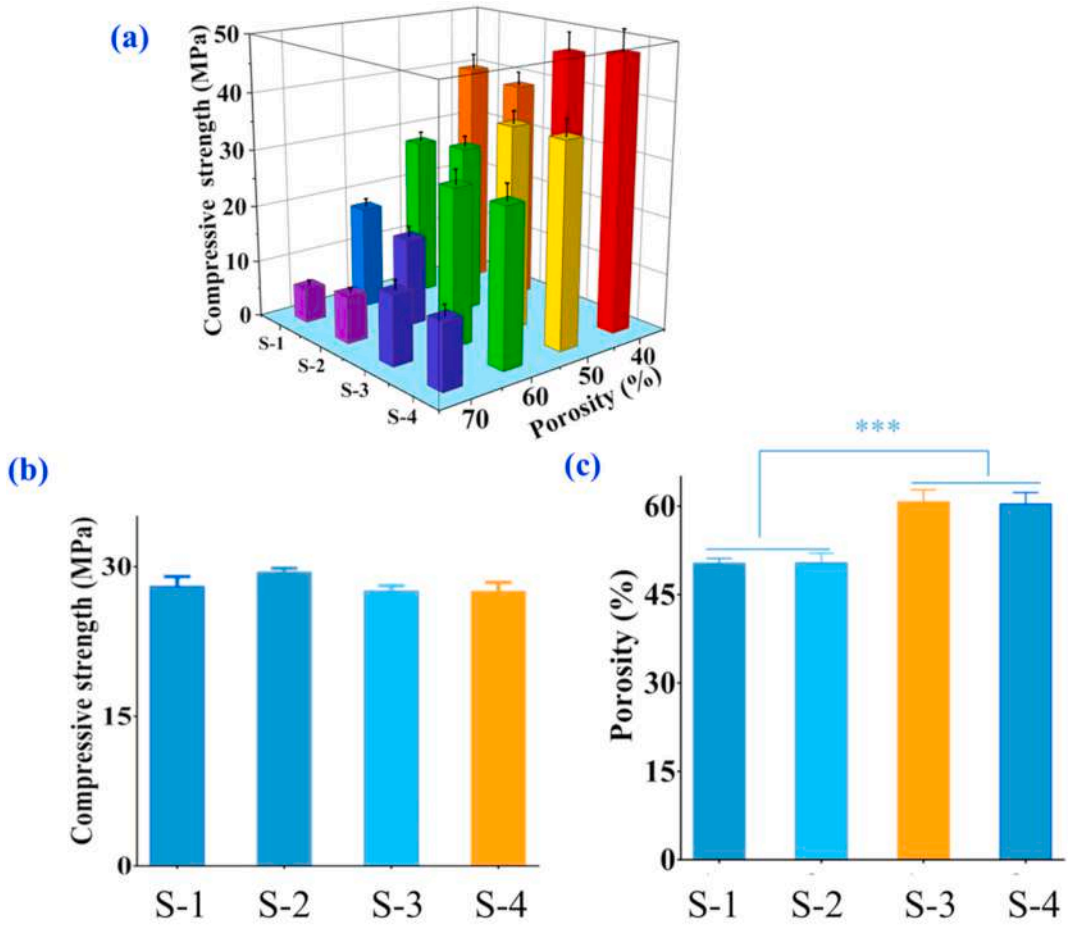


**Fig. 4.** Analysis of the mechanical properties (a) Compression strength of the scaffolds changing with porosity; Statistical analysis of S-1, S-2, S-3 and S-4 shown in Fig. 3 (b) Compressive strength (c) Porosity (***$p < 0.05$).

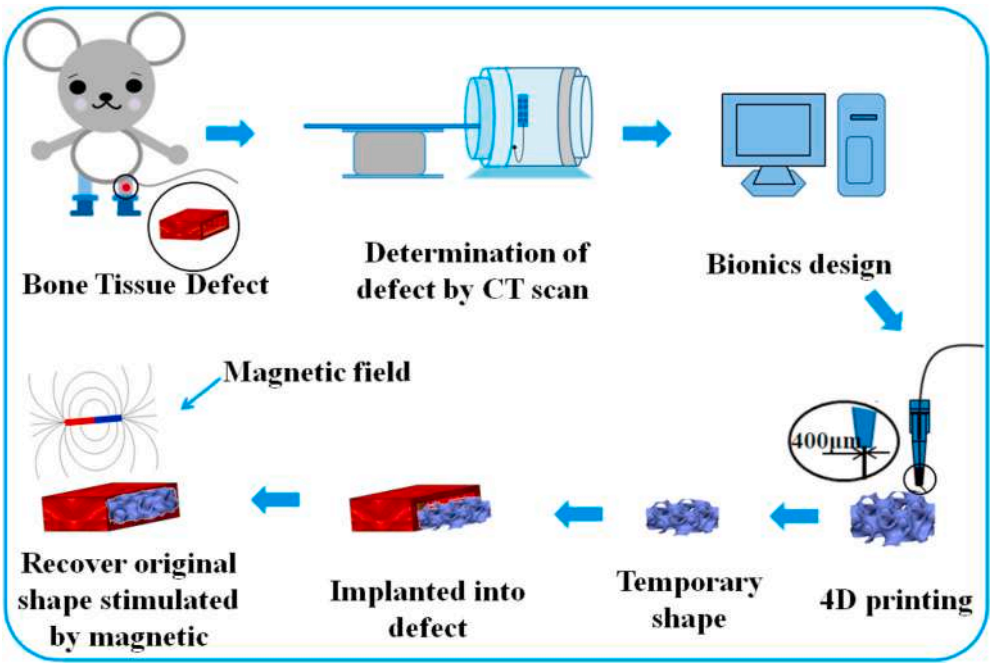


**Fig. 5.** Schematic of design, fabrication and implantation process of porous bone tissue structures.

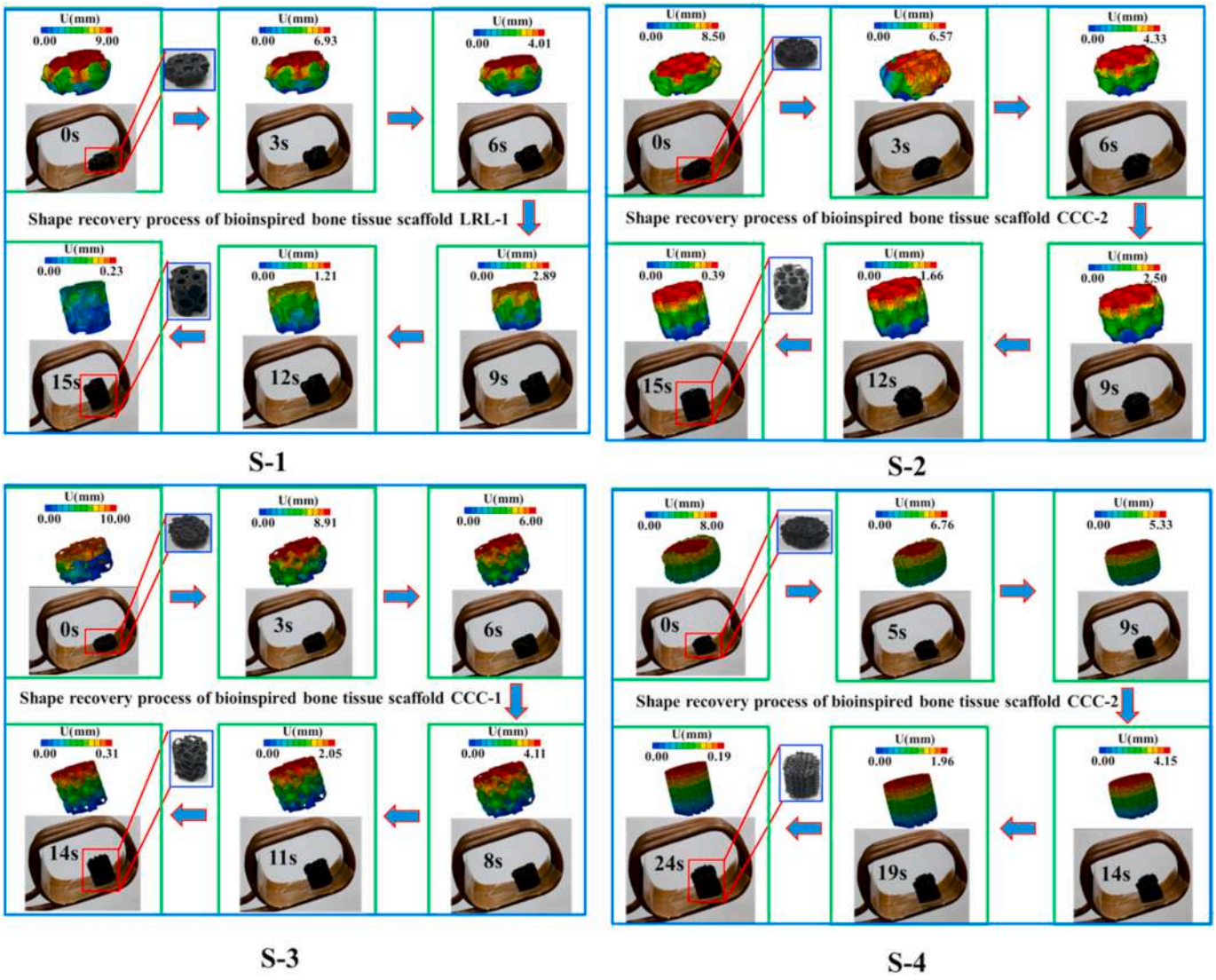


**Fig. 6.** Illustration of the shape recovery process by FEA and experiment for S-1, S-2, S-3 and S-4 (a) S-1 (b) S-2 (c) S-3 (d) S-4.

Because scaffolds S-1 and S-2 with the porosity of 50%, and S-3 and S-4 with the porosity of 60% were selected to investigate the osteogenesis effect, we performed a statistical analysis of the four scaffolds. For the scaffolds shown in Fig. 3, the compression strength of S-1 and S-2 (50% porosity) are 28 ± 0.8164 MPa and 29.43 ± 0.33 MPa, respectively, while the compressive strengths of S-3 and S-4 (60% porosity) are 27.53 ± 0.45 MPa and 27.5 ± 0.748 MPa, respectively. The compression strength of the four scaffolds has no statistical significance (Fig. 4(a), $p > 0.05$). The statistical analysis of the porosity is shown in Fig. 4(c), which indicates that the porosity has obvious statistical significance.

### 2.4. Working principle and functional verification

The schematic of the design, fabrication, and implantation process of the porous scaffold is illustrated in Fig. 5. Firstly, the specific configuration of the bone defect is obtained by a computed tomography (CT) scan. Secondly, the scaffolds are designed combined with bionics and fabricated by 3D printing. Subsequently, the scaffold is implanted into the body in a much smaller compact state than the bone defect. Finally, the scaffold recovers to its initial shape stimulated by the magnetic field. The minimally invasive implantation will greatly minimize unnecessary trauma.

Functional verification is carried out in vitro to verify the recovery performance of the porous scaffolds. The magnetic field is considered as the most elegant and potential actuation mechanism for the deployment of SMP based implantation device, which can realize non-contacting and remote actuation. Stimulated by the external magnetic field, the ferromagnetic nano-particles moves periodically as the magnetic field changes. The heat generated by relative friction and collision between ferromagnetic nano-particles and polymer molecules triggers the shape recovery of the scaffolds.

The scaffolds were firstly compressed into a compact state, and they recovered to their original shape stimulated by a 30 kHz alternating magnetic field. The shape recovery process for scaffolds S-1, S-2, S-3 and S-4 are shown in Fig. 6 (a)-(d). The comparison results of simulation and experiment illustrated the effectiveness and provide a foundation for application in minimally invasive orthopedics (Corresponding model parameters can be found in Supporting Information S1-S3). Exposed to the magnetic field for 15 s, 15 s, 14 s, and 24 s, S-1, S-2, S-3 and S-4 recover to their original shape, and the shape recovery ratio is higher than 95.5% (See Movies S1–S4 for the recovery effectiveness).

Supplementary video related to this article can be found at https://doi.org/10.1016/j.compscitech.2020.108563

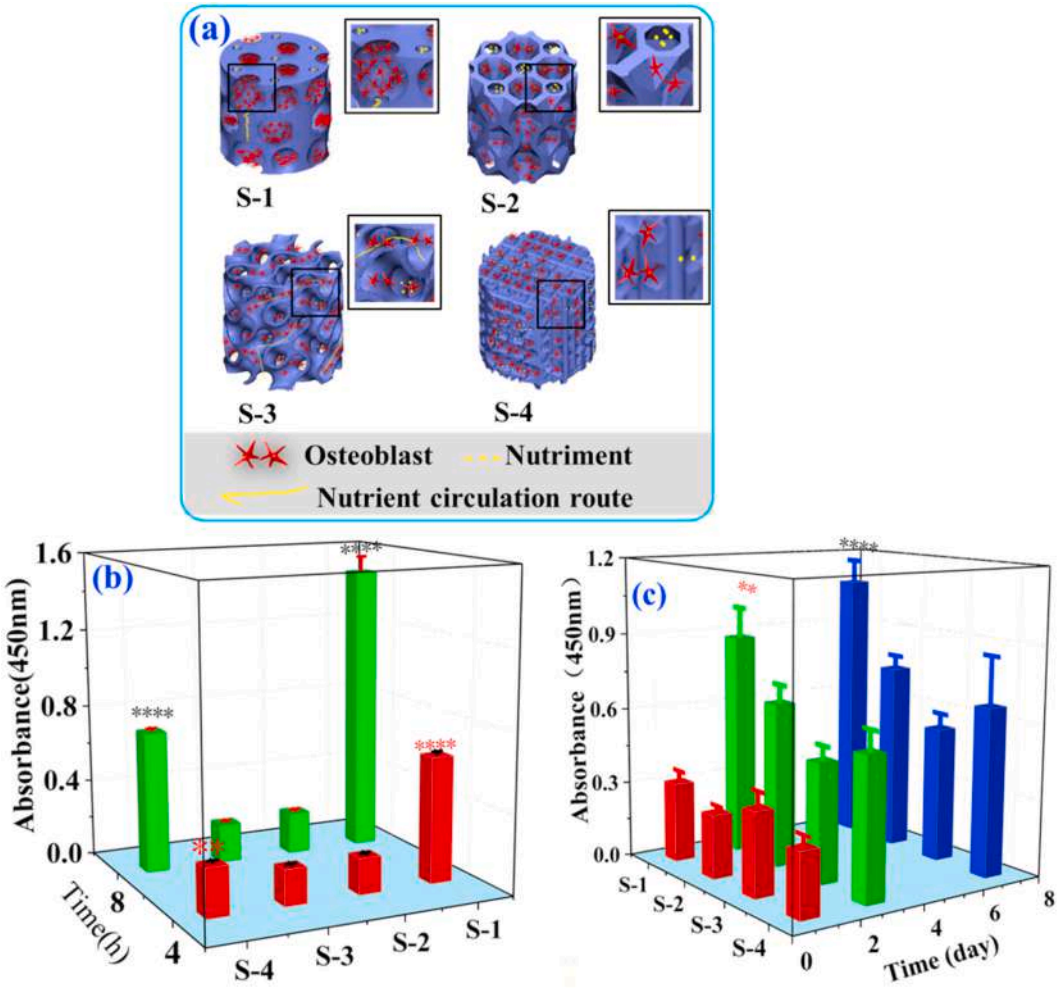


**Fig. 7.** Evaluation of biological activity (a) Schematic diagram of cell adhesion and nutrient transport on the scaffolds (b) Absorbance value of the cells cocultured with scaffolds for 4 h and 8 h (c) Absorbance value of cells cocultured with scaffolds for 1 d, 3 d and 7 d (Comparisons of S-1, S-2, S-3 and S-4; $^{**}p < 0.01$, $^{****}p < 0.0001$).

### 2.5. Evaluation of biological activity in vitro

Scaffolds S-1, S-2, S-3 and S-4 have different apertures, porosities and pore shapes, which exhibit different promotion effects on cell adhesion and proliferation. The schematic diagram of cell adhesion and nutrient transport on scaffolds are illustrated in Fig. 7(a). The pores with varying sizes not only provide space for the adhesion of the cell but also make the exchange of nutrients more convenient. Due to the large enough apertures, the probability of the main channel being blocked by the accumulation of cells is greatly reduced. To explore the cell adhesion effect, the osteoblast suspension is dripped into the scaffolds and cocultured with the scaffolds for 4 h, 8 h, 1 d, 3 d, and 7 d at 37°C, respectively (Experiment procedures can be found in Supporting Information S6.1). Statistical analysis indicates that the cells attached to the scaffolds increase significantly, as shown in Fig. 7(b). S-1 exhibits a better cell adhesion effect than S-2 ($p < 0.0001$), while the microstructure of S-4 is more beneficial for cell adhesion compared to S-3 ($p < 0.01$).

Furthermore, the proliferation of the osteoblasts with the delay of culturing time further verify the biocompatibility of shape memory PLA/$Fe_3O_4$ and the promotion effect of scaffolds on cell adhesion (Fig. 7(c)). However, the scaffolds have slightly different promotion effects on cell adhesion, which S-1 performs the best, followed by S-2, S-4, and S-3. For scaffolds S-1 and S-2, osteoblast proliferates dramatically with the extending of culturing time, while for scaffolds S-3 and S-4, there is no significant difference between the cells cocultured with the scaffolds for

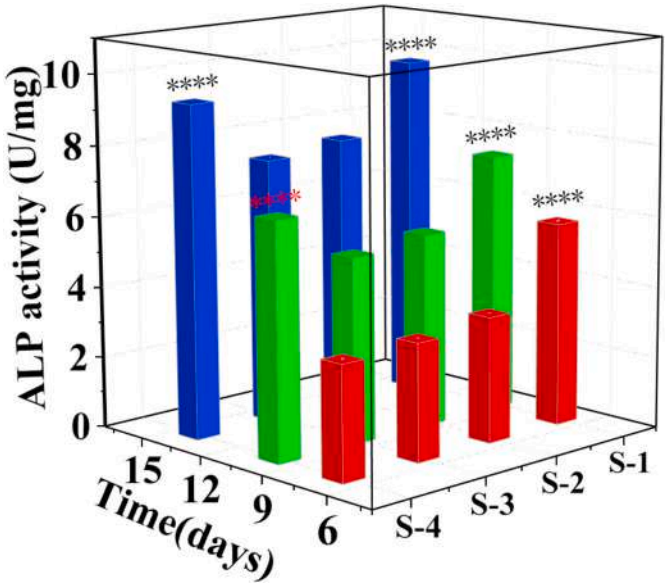


**Fig. 8.** Evaluation of the osteogenic effect (Comparison of S-1 and S-2, S-3 and S-4; $^{****}P < 0.0001$).

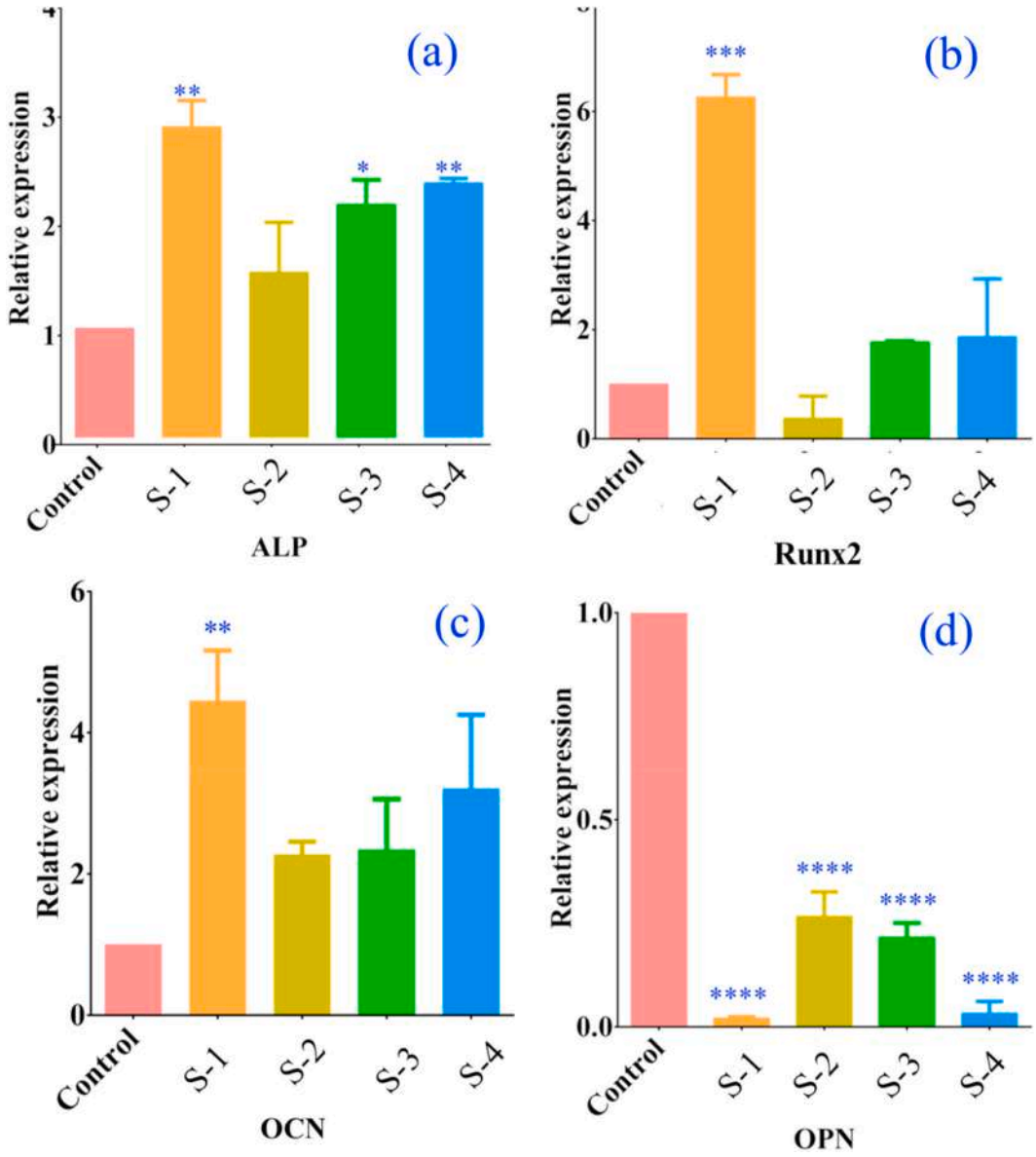


**Fig. 9.** Evaluation of osteogenic effect, expression levels of (a) alkaline phosphatase (b) Runt-related transcription factor 2 (c) Osteocalcin (d) Osteopontin. After 10 days of cocultivation. (One-way analysis of variance followed by Tukey post hoc; *p < 0.05; **p < 0.01, ***p < 0.001, ****p < 0.0001.)

3 d and 7 d. This phenomenon may be attributed to the fact that a scaffold equipped with both large and small pores are more conducive to cell adhesion and proliferation. The pores with small size are better for cell adhesion, and the pores with large size are more beneficial to the exchange of nutrients. In the long run, cell proliferation is easily restricted by nutrient deficiency due to the poor circulation of small pores. The attachment of osteoblast on the scaffolds is observed by a confocal laser scanning microscopy as shown in Figure S6.

### 2.6. Evaluation of osteogenic effect in vitro

To determine the osteogenic capacity, the osteoblasts are co-cultured with the scaffolds for 7 d, 10 d, and 14 d (Experiment procedures can be found in Supporting Information S6.2). Analysis results indicate that scaffold S-1 exhibits a better osteogenic capacity throughout the culture cycle compared with S-2, which is consistent with the results of CCK-8 (Fig. 8). On the seventh day, the osteogenic capacity of scaffolds S-3 and S-4 has no statistical significance. However, scaffold S-4 exhibits a more significant osteogenic effect in the tenth day and fourteenth day compared with S-3, which indicates a more durable osteogenic capacity. The results further verify that scaffolds equipped with both large and small pores exhibit a better ability to promote cell proliferation and adhesion. However, the influence of porosity cannot be excluded, and the potential mechanisms need to be further verified.

Bone formation goes through three main stages: the proliferation of osteoblasts, the maturation and mineralization of the extracellular matrix. The process of bone formation, including the production of alkaline phosphatase (ALP), processing of the procollagen and deposition of the extracellular matrix, is regulated by major cytokines, [37]. Furthermore, the differentiation of osteoblasts is strictly controlled by a variety of internal and external factors. The ALP, mainly distributed in the cell membrane, is produced to accelerate the maturation of osteoblast. Mineralization of the extracellular matrix is a marker that can be easily recognized to reflect the biochemical of osteoblasts' activity.

Real-time Polymerase chain reaction (RT-PCR) is utilized for the assessment of osteogenic related gene expression (Experiment procedures can be found in Supporting Information S6.3). In the early stage of osteoblast differentiation, the expression level of ALP increases (Fig. 9

(a)). Runt-associated transcription factor 2 (Runx2), binding to the promoter region, is the most critical transcription factor during this period to trigger the expression of ALP. The expression level of Runx2 with the cells culturing for 7 d is shown in Fig. 9(b) (Experiment procedures can be found in Supporting Information S6.4). The results indicate that the osteoblast seeded on S-1, S-2, S-3 and S-4 are up-regulated for 2.8, 1.5, 2.1 and 2.33 time than the blank control group. Moreover, the relative expression level of Runx2 of cells cocultured with scaffold S-1 is higher than that of cocultured with scaffold S-2 while there is no significance between scaffolds S-3 and S-4, which is consistent with the results mentioned above.

Osteocalcin (OCN) is a biomarker of osteoblasts differentiation in the later period, which indicates the deposition of extracellular matrix (ECM). Compared with the control group, the expression level of the OCN gene of cells cocultured with scaffold S-1 significantly increase ($p < 0.05$). The expression level of other groups is higher than the control group, but it is not statistically significant (Fig. 9(c)). OPN is a negative regulator to promote the proliferation and differentiation of MC3T3-E1 cells [38]. Evidence suggests that OPN stimulates the resorption activity of osteoclasts and promotes the maturation of osteoclasts [38]. As shown in Fig. 9(d), the expression levels of the osteopontin gene (OPN) of cells cocultured with the scaffolds are significantly lower than the control group ($p < 0.0001$). Consequently, it can be concluded that the expression level of the gene is inhibited to different degrees. Scaffolds S-1 and S-4 exhibit a better inhibit capacity on the expression of OPN. Moreover, the scaffolds S-1and S-2 are more beneficial to promote the adhesion, proliferation and osteogenesis at the early stage. Even though the scaffolds S-3 and S-4 exhibit good cell adhesion effect, no obvious cell proliferation effect is observed at the early stage. However, it is interesting that the promotion effect of scaffolds S-3 and S-4 on cell proliferation and osteogenesis is observed at the later stage. The potential mechanisms and signaling pathways need to be further studied.

## 3. Conclusions

In summary, this work introduces a series of porous bone tissue scaffolds based on SMPC that can be implanted into the body by minimally invasive surgery and recover to the work state stimulated by the magnetic field. The experimental and micromechanical theoretical studies verify the mechanical stability of the porous scaffolds. The biological experiments indicate that the porous scaffolds can greatly improve cell attachment and proliferation ability, which indicate its potential in cell delivery and bone regeneration. The shape memory effect indicates the scaffolds can deploy successfully stimulated by the magnetic field, which illustrates the potential application in the minimally invasive implant. Integrating porous structure into the design of bone tissue scaffolds and combining shape memory effect provides an alternative method for effective repair of bone defects.

## Declaration of competing interest

The authors declare that they have no known competing financial interests or personal relationships that could have appeared to influence the work reported in this paper.

## Acknowledgement

This work was supported by the National Natural Science Foundation of China (Grant No. 11632005, 11672086).

## Appendix A. Supplementary data

Supplementary data to this article can be found online at https://doi.org/10.1016/j.compscitech.2020.108563.

## References

[1] Z. Jamalpoor, H. Mirzadeh, M.T. Joghataei, D. Zeini, S. Bagheri-Khoulenjani, M. R. Nourani, Fabrication of cancellous biomimetic chitosan-based nanocomposite scaffolds applying a combinational method for bone tissue engineering, J. Biomed. Mater. Res. A 103 (5) (2015) 1882–1892.
[2] E. Gruskin, B.A. Doll, Demineralized bone matrix in bone repair: history and use, Adv. Drug Deliver. Rev 64 (12) (2012) 1063–1077.
[3] M. Spector, Biomaterials-based tissue engineering and regenerative medicine solutions to musculoskeletal problems, Swiss Med. Wkly. 137 (2006) 157–165.
[4] S.J. Hollister, Scaffold design and manufacturing: from concept to clinic, Adv. Mater. 21 (32–33) (2009) 3330–3342.
[5] A.J. Salgado, O.P. Coutinho, R.L. Reis, Bone tissue engineering: state of the art and future trends, Macromol. Biosci. 4 (8) (2004) 743–765.
[6] R.F. Service, Tissue engineers build new bone, Science 289 (5484) (2000) 1498.
[7] A. Gregor, E. Filova, M. Novak, J. Kronek, H. Chlup, M. Buzgo, V. Blahnova, V. Lukasova, M. Bartos, A. Necas, Designing of PLA scaffolds for bone tissue replacement fabricated by ordinary commercial 3D printer, J. Biol. Eng. 11 (1) (2017) 31.
[8] S.W. Choi, J.W. Xie, Y.N. Xia, Chitosan-based inverse opals: three-dimensional scaffolds with uniform pore structures for cell culture, Adv. Mater. 21 (29) (2009) 2997–3001.
[9] C.B. Ahn, Y. Kim, S.J. Park, Y. Hwang, J.W. Lee, Development of arginine-glycine-aspartate-immobilized 3D printed poly (propylene fumarate) scaffolds for cartilage tissue engineering, J Biomat Sci-Polym E 29 (7) (2018) 917–931.
[10] Y.Q. Mao, F. Chen, S.J. Hou, H.J. Qi, K. Yu, A viscoelastic model for hydrothermally activated malleable covalent network polymer and its application in shape memory analysis, J. Mech. Phys. Solid. 127 (2019) 239–265.
[11] H.B. Lu, X.D. Wang, X.J. Shi, Y.Q. Fu, K. Yu, A thermomechanical model of multi-shape memory effect for amorphous polymer with tunable segment compositions, Compos. Part B-Eng. 160 (2019) 298–305.
[12] W. Zhao, L.W. Liu, J.S. Leng, Y.J. Liu, Thermo-mechanical behavior prediction of particulate reinforced shape memory polymer composite, Compos. Part B: Eng. 179 (2019) 107455.
[13] D.W. Hanzon, H. Lu, C.M. Yakacki, K. Yu, Influence of mechanically-induced dilatation on the shape memory behavior of amorphous polymers at large deformation, Mech. Time-Depend. Mat. 23 (1) (2018) 1–21.
[14] A. Butscher, M. Bohner, S. Hofmann, Structural and material approaches to bone tissue engineering in powder-based three-dimensional printing, Acta Biomater. 7 (3) (2011) 907–920.
[15] W. Zhao, L.W. Liu, J.S. Leng, Y.J. Liu, Thermo-mechanical behavior prediction of shape memory polymer based on multiplicative decompositions of the deformation gradient, Mech. Mater. 143 (2019) 103263.
[16] M. Behl, M.Y. Razzaq, A. Lendlein, Multifunctional shape-memory polymers, Adv. Mater. 22 (31) (2010) 3388–3410.
[17] W. Zhao, Q. Wang, L.W. Liu, Y.J. Liu, J.S. Leng, Structural response measurement of shape memory polymer components using digital image correlation method, Opt. Laser. Eng. 110 (2018) 323–340.
[18] M. Herath, J. Epaarachchi, M. Islam, F.H. Zhang, J.S. Leng, L. Fang, C. Yan, G. D. Peng, W. Schade, Remote actuation of light activated shape memory polymers via D-shaped optical fibers, Smart Mater. Struct. 29 (2020), 047001.
[19] M. Herath, J. Epaarachchi, M. Islam, C. Yan, F.H. Zhang, J.S. Leng, Effects of selectively triggered photothermal particles on shape memory polymer composites: an investigation on structural performance, thermomechanical characteristics and photothermal behavior, J. Intel. Mat. Syst. Str. 30 (20) (2019) 3124–3135.
[20] W. Zhao, L.W. Liu, F.H. Zhang, Y.J. Liu, J.S. Leng, Shape memory polymers and their composites in biomedical applications, Mat. Sci. Eng. C-Mater. 97 (2019) 864–883.
[21] W. Zhao, L.W. Liu, X. Lan, Y.J. Liu, J.S. Leng, Adaptive repair device concept with shape memory polymer, Smart Mater. Struct. 26 (2) (2017), 025027.
[22] W. Zhao, F.H. Zhang, Y.J. Liu, J.S. Leng, Personalized 4D printing of bioinspired tracheal scaffold concept based on magnetic stimulated shape memory composites, Compos. Sci. Technol. 184 (2019) 107866.
[23] Q.L. Zhao, J. Wang, Y.L. Wang, H.Q. Cui, X.M. Du, A stage-specific cell-manipulation platform for inducing endothelialization on demand, Natl. Sci. Rev. 7 (3) (2020) 629–643.
[24] Q.L. Zhao, J. Wang, H.Q. Cui, H.X. Chen, Y.L. Wang, X.M. Du, Programmed shape-morphing scaffolds enabling facile 3D endothelialization, Adv. Funct. Mater. 28 (2018) 1801027.
[25] J. Wang, Q.L. Zhao, Y.L. Wang, Q. Zeng, T.Z. Wu, X.M. Du, Self-unfolding flexible microelectrode arrays based on shape memory polymers, Adv. Mater. Technol. (2019) 1900566.
[26] F.P.W. Melchels, M.A.N. Domingos, T.J. Klein, J. Malda, P.J. Bartolo, D. W. Hutmacher, M. Domingosc, T. Klein, Additive manufacturing of tissues and organs, Prog. Polym. Sci. 37 (8) (2012) 1079–1104.
[27] S. Tibbits, 4D printing: multi-materials shape change, Architect. Des 84 (1) (2014) 116–121.
[28] Q. Ge, H.J. Qi, M.L. Dunn, Active materials by four-dimension printing, Appl. Phys. Lett. 103 (13) (2013) 131901.
[29] M. Lei, W. Hong, Z. Zhao, C. Hamel, M.J. Chen, H.B. Lu, H.J. Qi, 3D printing of auxetic metamaterials with digitally reprogrammable shape, ACS Appl. Mater. Inter. 11 (25) (2019) 22768–22776.
[30] R. De Santis, U. D'Amora, T. Russo, A. Ronca, A. Gloria, L. Ambrosio, 3D fibre deposition and stereolithography techniques for the design of multifunctional nanocomposite magnetic scaffolds, J Mater. Sci-Mater. M. 26 (10) (2015) 250.

[31] B.C. Gross, J.L. Erkal, S.Y. Lockwood, C.P. Chen, D.M. Spence, Evaluation of 3D printing and its potential impact on biotechnology and the chemical sciences, Anal. Chem. 86 (2014) 3240–3253.
[32] Y. Zhang, Post-printing surface modification and functionalization of 3D-printed biomedical device, International Journal of Bioprinting 3 (2) (2017) 93–99.
[33] P.A. Guntillake, R. Adhikari, Biodegradable synthetic polymers for tissue engineering, Eur. Cell. Mater. 5 (1) (2003) 1–16.
[34] P.R. Buckley, G.H. McKinley, T.S. Wilson, W. Small, W.J. Benett, J.P. Bearinger, M. W. McElfresh, D.J. Maitland, Inductively heated shape memory polymer for the magnetic actuation of medical devices, IEEE T. Bio-Med. Eng. 53 (10) (2006) 2075–2083.
[35] P.R. Stauffer, T.C. Cetas, A.M. Fletcher, D.W. DeYoung, M.W. Dewhirst, J. R. Oleson, R.B. Roemer, Observations on the use of ferromagnetic implants for inducing hyperthermia, IEEE T. Bio-Med. Eng. 1 (1984) 76–90.
[36] A. Jordan, P. Wust, H. Fahling, W. John, A. Hinz, R. Felix, Inductive heating of ferrimagnetic particles and magnetic fluids: physical evaluation of their potential for hyperthermia, Int. J. Hyperther. 25 (7) (2009) 499–511.
[37] P. Magnusson, L. Larsson, M. Magnusson, M.W.J. Davie, C.A. Sharp, Isoforms of bone alkaline phosphatase: characterization and origin in human trabecular and cortical bone, J. Bone Miner. Res. 14 (1999) 1926–1933.
[38] J.H. Zhou, B. Li, S.M. Lu, L. Zhang, Y. Han, Regulation of osteoblast proliferation and differentiation by interrod spacing of Sr-HA nanorods on microporous titania coatings, ACS Appl. Mater. Inter. 5 (11) (2013) 5358–5365.